Pergamon

Cement and Concrete Research 33 (2003) 197–206

CEMENT AND CONCRETE RESEARCH

Characterization and monitoring of cement-based systems using intrinsic electrical property measurements

W.J. McCarter*, T.M. Chrisp, G. Starrs, J. Blewett

Department of Civil and Offshore Engineering, Heriot Watt University, Edinburgh EH14 4AS, Scotland, UK

Received 17 January 2002; accepted 3 April 2002

Abstract

This paper highlights the application of electrical property measurements as a characterization and investigative technique in the study of cementitious systems at the micro- and macroscale. Both fixed-frequency and spectral measurements are exploited to study cement pastes, mortars and concretes and results are presented from research programs relating to the early hydration of cement-based systems, characterization of fly ash, and concrete durability. The work comprises both laboratory-based investigations and field-monitoring studies. The methodology could complement other techniques that are used in the study of cement-based materials.
© 2002 Elsevier Science Ltd. All rights reserved.

Keywords: Cement; Concrete; Characterization; Electrical properties; Durability

1. Introduction

Concrete and other cement-based systems now dominate the built environment, having become some of the world's most important construction materials. Although the manufacture of Portland cement (PC) is energy intensive, it continues to be the main cementitious component in concrete, although the performance enhancing characteristics of blended cementitious systems have a role to play in the design of concrete structures for minimum maintenance/repair. Indeed, the use of alternative cementitious binders, produced from the by-products of traditional industries, will help in reducing energy consumption and CO_2 emission, and, in this way, lead to more sustainable construction materials. It is also recognised that alkali additions can activate pozzolanic materials to set and harden in their own right and there is considerable scope for the development of PC-free binders.

Cementitious systems (comprising pastes, mortars and concretes) must be studied and understood at the submicroscopic and microscopic levels, where length scales are measured in terms of Angstroms and microns, through to the macroscale, where length scales are of the order of centimetres and metres (i.e., bulk concrete). It is set against this background that the current paper reviews and outlines the application of the intrinsic electrical properties of cementitious systems as a testing methodology to study and evaluate these materials at both the micro- and macroscale. As way of illustration, results are presented for studies relating to (a) the early hydration of cementitious systems, (b) characterisation of fly ash, and (c) concrete-durability studies. Both fixed-frequency and spectral measurements are exploited.

2. Experimental studies

Details relating to the theory of ac electrical property (EP) measurements on cementitious systems are well documented (see Refs. [1–10], for example) and this aspect will not be discussed in detail; suffice to state that the electrical response of a material contained between a pair of electrodes at frequency, f, of applied electrical field can be written as:

$$Y(f) = G(f) + j2\pi fC(f)$$

where $G(f)$ and $C(f)$ represent, respectively, the conductance and capacitance of the complex admittance, $Y(f)$,

* Corresponding author. Tel.: +44-131-451-3318; fax: +44-131-451-5078.

E-mail address: johnm@civ.hw.ac.uk (W.J. McCarter).

0008-8846/02/$ – see front matter © 2002 Elsevier Science Ltd. All rights reserved.
PII: S0008-8846(02)00824-4

at frequency f hertz (Hz), and $j = \sqrt{-1}$. The complex impedance, $Z(f)$, is the reciprocal of $Y(f)$. Ionic conduction and losses resulting from relaxation of polarization processes will be quantified by G, whereas polarization mechanisms operative within the system are quantified by the capacitance, C [11].

2.1. Early hydration of cementitious systems

The reaction kinetics of PC and pozzolanic materials activated with a suitable alkali are traditionally studied using isothermal calorimetry techniques [12,13]. The work presented below utilizes EP measurements as a viable method for studying this reaction and also highlights the potential use of the testing methodology for monitoring pozzolanic reactivity of by-products and cementitious materials generally.

Results are presented for the following:

(a) ground granulated blast-furnace slag (GGBS) activated with sodium silicate;
(b) GGBS activated with calcium hydroxide (CH); and
(c) a PC paste.

GGBS used in the current work had a composition: 41.2% CaO; 35.1% SiO_2; 12.0% Al_2O_3; 8.5% MgO; 0.3% Fe_2O_3; 0.17% Na_2O; 0.43% K_2O; LOI = 0.45%. Reagent grade sodium silicate (NS), having an SiO_2/Na_2O ratio of 2.0 (i.e., modulus), and CH were used as activators. GGBS was mixed with the activator in the ratio 4:1 (by mass) with a water/solids ratio of 0.4 (by mass). PC (ASTM Type I) of composition 63.9% CaO; 26.7% SiO_2; 4.83% Al_2O_3; 2.53% MgO; 3.17% Fe_2O_3; 0.08% Na_2O; 0.54% K_2O; LOI 0.77% was used, with a water/PC ratio of 0.27.

After mixing with distilled water, the pastes were compacted into Plexiglas test cells of internal dimensions $50 \times 50 \times 50$ mm. Two opposite walls of the cells had 50×50 stainless steel plate electrodes, which were connected to an impedance analyser. Samples were covered with a Plexiglas sheet and placed in small Perspex cabinets, which maintained a humidity of $\approx 90\%$ (20 ± 1 °C). The change in sample conductance, G (reciprocal of resistance), and capacitance, C, were studied over the frequency range 1–100 kHz. A personal computer was used for automatic data logging with measurements taken every 10 min over the 48-h test period, although for clarity only every third data marker is highlighted on the figures.

2.1.1. Results and discussion

Fig. 1(a) presents a typical conductance versus time curve for the GGBS/NS mixture at a frequency of 100 kHz; also presented on this figure is the derivative of the con-

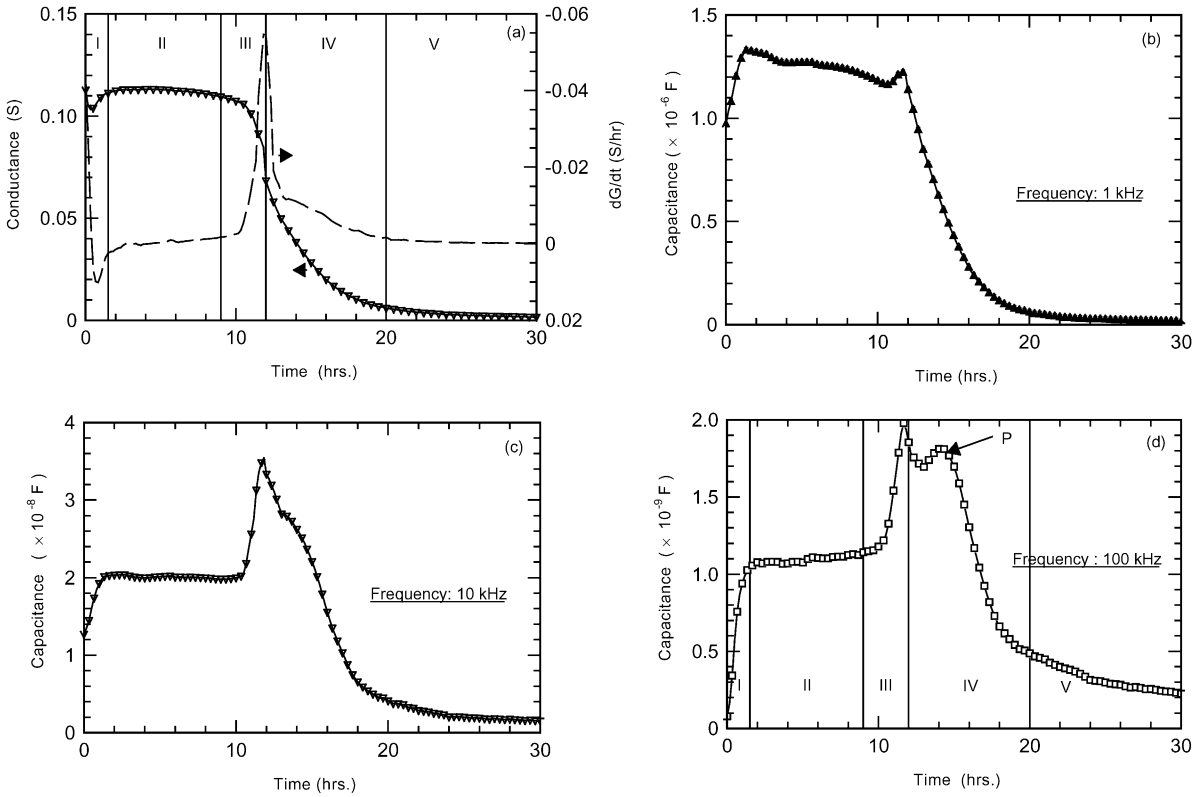

Fig. 1. (a) Conductance (and derivative) versus time for GGBS/NS mixture with regions I–V indicated; capacitance versus time response at a frequency of (b) 1, (c) 10 and (d) 100 kHz.

ductance curve, dG/dt (dashed line). Since the conductance will reflect the increase in rigidity of the mixture, its derivative must give an assessment of the rate of chemical activity occurring within the system. Considering both curves, it is evident that the responses can be divided into several distinct regions and indicated I–V in this figure. An initial region, designated I, extending from the start of the test up to approximately 1 h. From 1 to 9 h, there is a region where there is little change in conductance and would indicate a period of reduced chemical activity within the mixture (II). Over the period 9–12 h, the conductance undergoes a rapid reduction and would imply a period of intense chemical activity where the rigidity of the mixture increases (III). From 12 to 20 h, the rate of change of conductivity reduces, indicating a reduction in the intensity of chemical activity (IV). From 20 h onwards, there is a general slowing down in reaction rate, which would be indicative of gradual infilling and accretion of hydration products (V).

Parallels can obviously be drawn with isothermal conduction calorimetry studies used to identify the sequence of PC hydration, viz. a preinduction period (Stage I); a dormant period (Stage II); an acceleratory period (Stage III); deceleration period (Stage IV), followed by the slower, diffusion controlled period (Stage V). It should be emphasised that the tests above were not conducted under isothermal conditions.

Fig. 1(b)–(d) displays the change in capacitance for the GGBS/NS mixture at 1, 10 and 100 kHz, respectively. Over the two decades of frequency represented by these figures, the sample capacitance can reduce by almost three orders of magnitude highlighting the frequency dependence of this parameter and also indicating a region of dielectric dispersion. The capacitance is a measure of the sum of all the polarization processes operative within the system at that particular frequency; for example, a polarization process (or processes) operative at the lowest frequency may be considerably reduced or even eliminated at the highest frequency. It is evident from Fig. 1(c) and (d), that not only do the absolute values of capacitance change markedly, but the profile of the response at each frequency also changes significantly. Certain detail in the response only becomes apparent at frequencies in excess of 10 kHz where a prominent peak in capacitance dominates the central portion of the curve. At the lowest frequency presented (1 kHz), electrode polarization processes will have a dominant influence on the measured capacitance of the system and mask the bulk response from the paste. However, as the frequency increases, the contribution from electrode processes reduces, thereby revealing the polarization response from the bulk mixture. The sudden increase in polarizability of the mixture must indicate either a phase change or transformation, or increase in surface area of the products of hydration and discussed below.

The regions identified from the conductance response, and its derivative, have been transferred onto Fig. 1(d). It is interesting to observe that the peak in capacitance occurs at the same time at which dG/dt maximises and which delineates regions III and IV. It is over these periods that the mixture undergoes a rapid increase in rigidity. In order to explain this feature the following are postulated. A rapid outgrowth of products of hydration (gel) from the grain surface into the aqueous phase would cause an increase in gel surface area; double-layer polarization processes, operative on the gel surface, would thus increase thereby increasing the polarizability of the paste. Alternatively (or in combination with the latter), the introduction of thin 'resistive' outgrowths from the grain surface into the pore water could cause an increase in polarizability of the system through an interfacial/Maxwell–Wagner [11] process, and the concept of dielectric amplification could also be invoked to account for such behaviour [7,8]. The peak is only transitory as infilling and accretion of the pore space with hydration products will reduce the polarizability of the system and result in a reduction in capacitance values.

For comparative purposes, the conductance and its derivative, and capacitance values for GGBS activated with CH are presented in Fig. 2(a) and (b), respectively. Electrical measurements are presented at 100 kHz. The regions I–V discussed above are detected and indicated on Fig. 2(a), although it is evident that the duration of Stages I–IV have increased in comparison to the GGBS/NS mixture. The derivative curve also indicates a more sluggish reaction rate and is confirmed by the capacitance response, as the prominence of the central peak is diminished in comparison the GGBS/NS mixture.

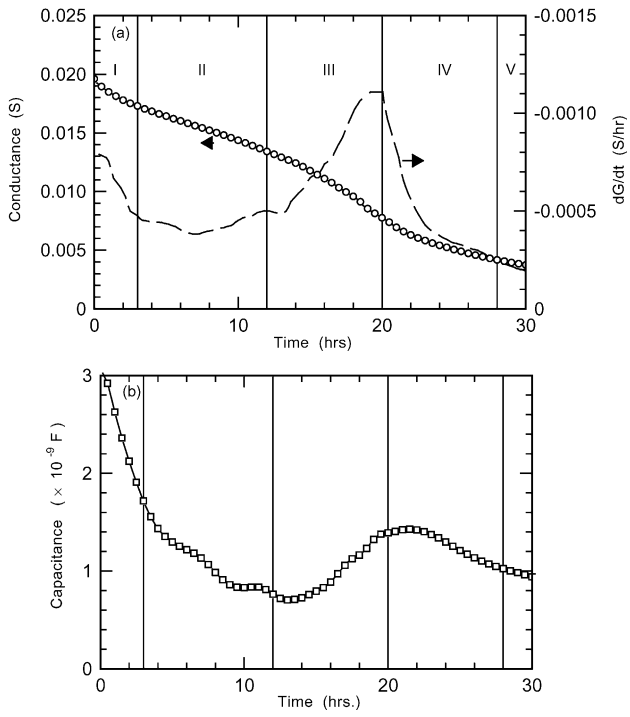

Fig. 2. (a) Conductance (and derivative) versus time for GGBS/CH mixture and, (b) capacitance versus time response at a frequency of 100 kHz.

Fig. 3(a) and (b) present the respective curves for PC paste over the initial 15-h hydration and at a frequency of 100 kHz. Again, the features identified above are present; the main difference being the duration of Stages I–IV, although it is evident that the absolute values of conductance, dG/dt and capacitance are similar to the GGBS/NS mixture. Due to the nature of the polarization process, which causes the increase in capacitance at setting (possibly an interfacial effect which relaxes in the MHz region), it would be anticipated that the prominence of the peak in capacitance would also reduce and eventually become undetectable at very high frequencies, as has been observed in PC/GGBS mixtures tested at frequencies in the microwave region [14].

Another feature which is detected in the capacitance response for both the PC and the GGBS/NS mixtures (Figs. 1(d) and 3(b) respectively), is the occurrence of a minor secondary peak after the initial main peak and indicated P on the figures. This could indicate a further phase transition and work is continuing in this respect.

2.2. Impedance of fly ash (FA) mixtures

Fly ash has an important role to play in the design of durable cementitious systems and, for the foreseeable future, extensive use will be made of this material. Characterization of fly ash is thus of importance, not only because of its widespread use, but also because the amount and quality of FA added to the binder is, ultimately, a decisive parameter in the performance of the concrete. EP measurements

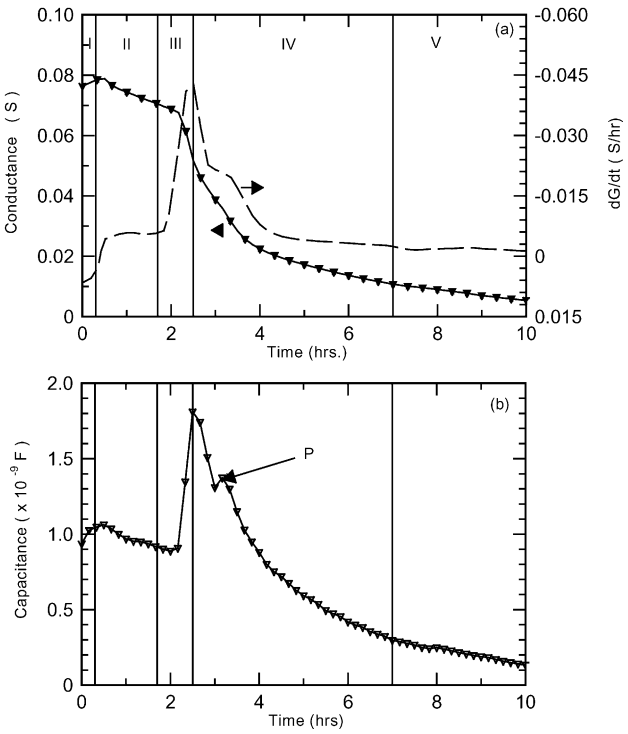

Fig. 3. (a) Conductance (and derivative) versus time for PC paste and (b) capacitance versus time response at a frequency of 100 kHz.

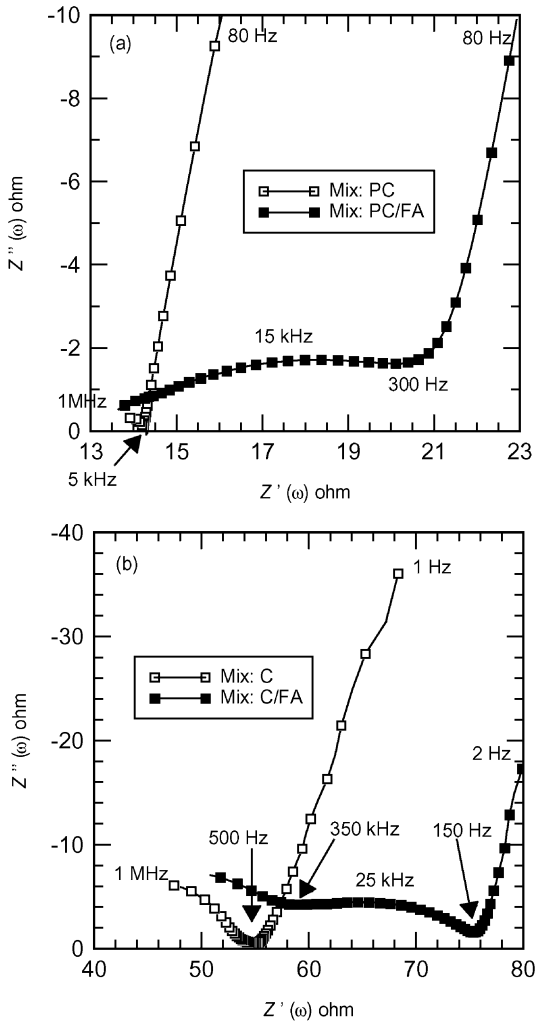

Fig. 4. Complex impedance response for (a) pastes: PC and PC/FA and (b) concrete mixes: C and C/FA. All measurements taken approximately 60 min after mixing.

on fly ash systems offer the possibility as a characterization technique.

Fig. 4(a) and (b) presents the complex impedance plots for PC paste and concrete specimens, with and without FA replacement. The composition of each mixture is given in Table 1 with PC (ASTM Type I) and BS 3892: Part 1 [15] fly ash (ASTM Class F) used throughout. The test cell for the paste samples had similar dimensions to that used in the tests above; the cells for the concrete samples had internal dimensions 150 × 150 × 150 mm with 150 × 150-mm stainless steel plate electrodes attached to two opposite faces of the cell. Electrical measurements are presented approximately 60 min after mixing over the frequency range 1 Hz–1 MHz.

2.2.1. Results and discussion

The specimens with plain PC binder display a typical two-region response comprising an electrode polarization spur and bulk arc to the right and left, respectively, of the cusp

point on the plot. The bulk arc is only partially developed due to the upper frequency limit of 1 MHz. The specimens with FA addition display a plot that is now characterized by three distinct zones: (i) the electrode response, (ii) a *plateau* region and (iii) a high-frequency arc. The dielectric constant and conductivity can be de-imbedded from the impedance data and the resulting dielectric and conductivity dispersion curves plotted in the frequency domain. These are presented in Fig. 5(a) and (b) for the curves in Fig. 4(a) and (b) respectively. The decrease in dielectric constant and rise in conductivity with increasing frequency is indicative of a region of dispersion resulting from relaxation of a polarization process within the system. At frequencies below, approximately, 1 kHz for pastes and 100 Hz for concretes, the dielectric constant rises to extremely high values and is attributed to the increasing influence of electrode polarization processes.

The inclusion of FA in the binder results in an enhancement of the bulk polarization processes in comparison to the plain PC mixtures, particularly over the range 10 kHz–1 MHz for both pastes and concretes. Further evidence can be obtained from the conductivity dispersion curves. The conductivity curves can be divided into two regions above and below 1 kHz (approximately). Below 1 kHz, and particularly over the region 1–100 Hz, the sharp increase in conductivity with increasing frequency is as a result of the reduction in electrode effects (as noted above from the dielectric dispersion data). At frequencies in excess of 1 kHz, there is a more gradual rise in conductivity with increasing frequency; of particular interest is that the dispersion in conductivity is more apparent in the mixtures with FA addition. The frequency range over which the increase in conductivity occurs is the same as that for the dielectric enhancement effect of the FA.

The increase in conductivity with increasing frequency of applied field is as a direct result of relaxation of the polarization mechanism, which, in addition to ionic conduction effects will contribute to loss processes. The overall result will be an increase in measured conductivity. With reference to Fig. 6 [16], a double-layer polarization process on the grain surface could be invoked to account for such a response. It is postulated that the enhancement of this process in the FA systems is due to the distinctive spherical nature of the FA particle.

To further highlight the existence of this feature, four (BS3892: Part 1) ashes from different sources within the United Kingdom (denoted UK: D/R/E/L) were tested and

Table 1
Summary of mixes for fly ash study

Mix	PC (kg/m^3)	FA (kg/m^3)	Fines (kg/m^3)	Coarse (kg/m^3)	Water (l/m^3)
PC	1619	–	–	–	485
PC/FA	881	587	–	–	440
C	405	–	608	1217	183
C/FA	237	158	593	1186	178

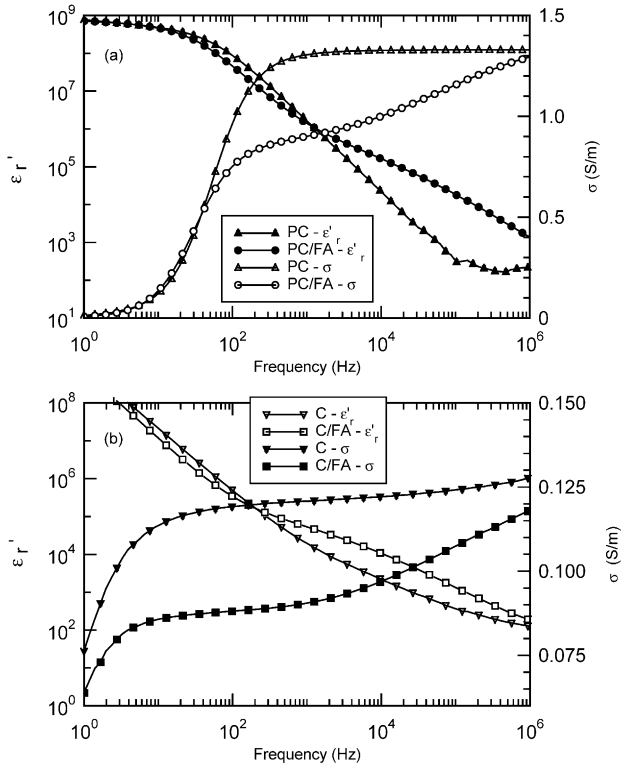

Fig. 5. Conductivity and dielectric dispersion curves for (a) pastes: PC and PC/FA and (b) concrete mixes: C and C/FA.

whose compositions were within the limits presented in Table 2; a Canadian ASTM Type F ash (denoted Can) was also tested. In this instance, the individual ashes were blended with hydrated lime in the ratio 4:1 and mixed with a water/solids ratio of 0.4; measurements were taken over the frequency range 1 Hz–10 MHz. Fig. 7(a) and (b) presents typical results for the ashes, tested approximately 30 min after mixing with water. The plateau region is present in all responses, although the ash in Fig. 7(b) is more resistive and the plateau is a very flat circular arc.

Clearly, electrical impedance methods could be further developed and exploited to characterize and detect FA in fresh concrete. A flotation technique [17] has been investigated for FA determination in fresh concrete but has been found to be too complex, not particularly suited for site application, and only useful as a laboratory method using skilled operatives. The same reference states "... it is astonishing to note that no method yet exists, which allows determination of fly-ash content in fresh concrete."

2.3. Concrete durability studies

The work below details the application of fixed-frequency (5 kHz) electrical conductivity measurements taken at discrete depths within the concrete cover (i.e., the cover-crete) to study water and ionic movement within this zone of concrete. The current study, which forms part of a long-term durability-monitoring program, presents data from

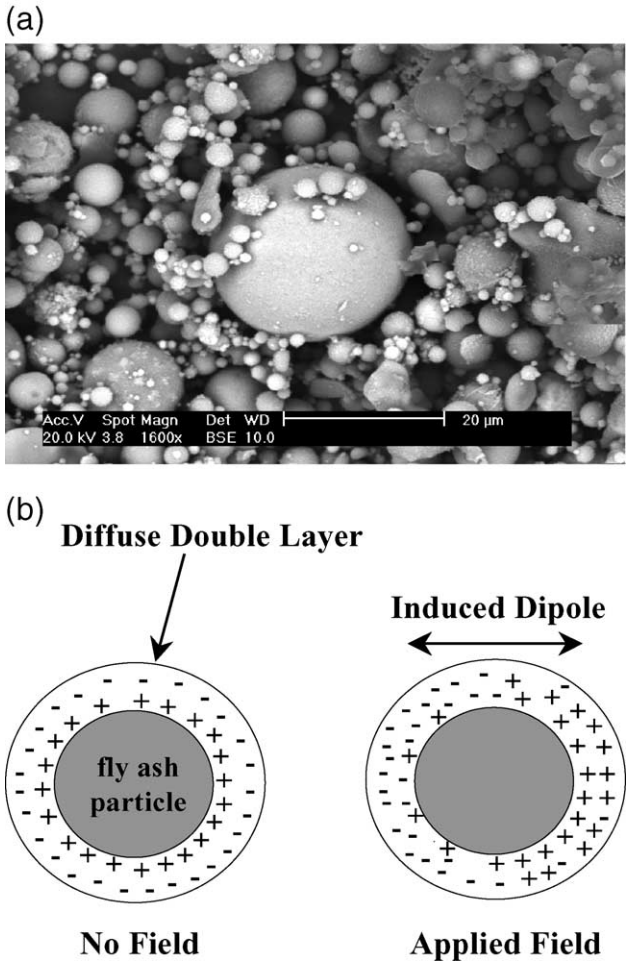

Fig. 6. Fly ash particles (top) and schematic diagram to illustrate a double-layer polarization process on particle surface.

laboratory specimens and specimens placed at a marine exposure site.

2.3.1. Materials and sample preparation

Laboratory specimens were 300 × 300 × 125 mm (thick) concrete blocks, cast in plywood formwork which had been given a coating of a proprietary release agent. Table 3 presents the mix details of the samples, together with the mean 7- and 28-day compressive strength (F_7 and F_{28}); dredged river coarse and aggregate was used throughout. Six samples were cast for each mix and each sample set was divided equally with one subset of specimens exposed to wetting cycles with water and the other subjected to wetting cycles of 1 M NaCl (1.0 M: 58.5 g/l). After demolding and curing under damp hessian and polythene for 7 days, the samples were sealed on the sides and top (i.e., trowelled) surface. The working (exposed) surface was that cast against the plywood formwork. Specimens were left in the laboratory (≈20 °C; 50–55% RH) for a period of 6 weeks before testing. Wetting and drying cycles comprised ≈48 h absorption followed by a period of drying, (generally ≈7 weeks). For the marine site, samples were 300 × 300 × 200 mm (thick) blocks. After demoulding, curing and sealing as above, the samples were left in the laboratory for a period of 3 weeks before transportation to the marine site.

Each specimen had a multielectrode array embedded within the covercrete allowing electrical resistance measure-

Table 2
Physical properties and oxide analysis (range) of BS3892: Part 1 ashes

	FA
Physical properties	
Specific gravity	2–2.4
Fineness: % retained on 45-μm sieve	<12%
Chemical analysis, %	
SiO_2	45–51
Al_2O_3	27–32
Fe_2O_3	7–11
CaO	1–5
MgO	1–4
TiO_2	0.8–1.1
SO_3	0.3–1.3
K_2O	1–5
Na_2O	0.8–1.7
LOI	<7

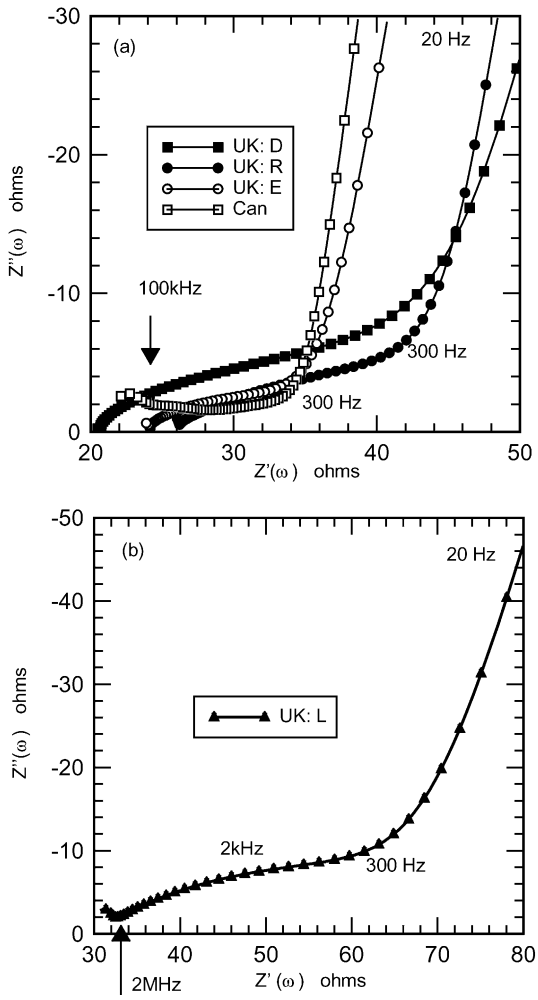

Fig. 7. (a) and (b) Complex impedance response for fly ash from different sources showing distinctive plateau region.

Table 3
Summary of mixes for concrete durability program

Mix	PC (kg/m^3)	FA (kg/m^3)	GGBS (kg/m^3)	20 mm (kg/m^3)	10 mm (kg/m^3)	Fines (kg/m^3)	WRA (l/m^3)	w/b	F_{7days} (MPa)	F_{28days} (MPa)
PC	460	–	–	700	350	700	1.84	0.4	57	70
GGBS	270	–	180	700	375	745	3.60	0.44	31	53
FA	370	160	–	695	345	635	2.65	0.39	33	58

WRA = water reducing agent; w/b = water–binder ratio, F = compressive strength at age indicated.

ments (hence its reciprocal, conductance) to be evaluated at 5-mm intervals through the surface 50 mm. Also mounted on each array were four thermistors, thereby allowing evaluation of temperature profiles with the covercrete. Details of the covercrete electrode array have been presented elsewhere [18,19]. The array was calibrated to allow conversion of conductance measurements to conductivity.

2.3.2. Results and discussion

For illustrative purposes, results are only presented for the Mixes 1 and 3 in Table 3. All conductivity values have been standardised to a reference temperature of 20 °C [20].

2.3.2.1. Laboratory specimens. Figs. 8 and 9 present the results for, respectively, water and NaCl solution applied at the exposed surface of the concrete specimens; only the response from depths of 5, 10, 15, 30 and 50 mm is displayed on these figures and only every third data marker is highlighted. As water is drawn into the partially saturated cover zone by capillarity, the wetting portion of the cycle is clearly evident and is characterized by an increase in conductivity, although the prominence of this increase diminishes with increasing depth and time. Where conductivity values increase, signifies that the wetting front has penetrated into the zone of influence of the electrical field between that particular electrode pair. Comparing Fig. 8 and Fig. 9, the influence of NaCl in the invading water is also detected as conductivity values over the surface 0–10 mm are enhanced in comparison to their water-exposed counterparts.

The influence of drying and wetting effects diminish with depth and the electrode pair at 50 mm displays little marked response to wetting and drying regime applied at the surface, showing a general decrease in conductivity with time over the test period presented. The latter is attributed to

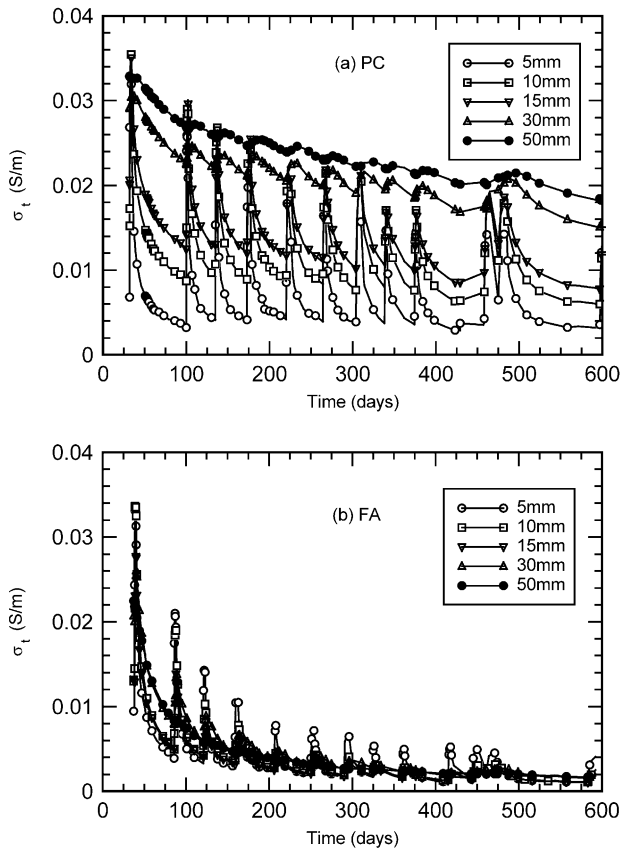

Fig. 8. Change in conductivity during cyclic wetting and drying with water applied at the exposed surface for (a) PC mix and (b) FA mix.

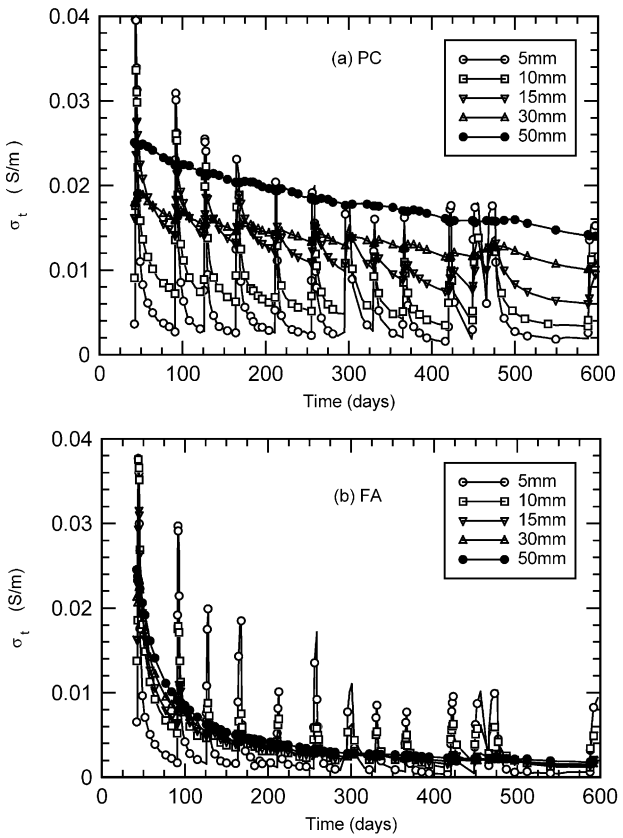

Fig. 9. Change in conductivity during cyclic wetting and drying with 1.0 M NaCl solution applied at the exposed surface for (a) PC mix and (b) FA mix.

ongoing hydration and pozzolanic reaction, indicating the continual refinement in pore structure within the cover zone. This effect is particularly evident in the FA mix; regarding this mix, the conductivity at 50 mm decreases by more than an order of magnitude between the first and last cycles. Furthermore, at any particular point in time, conductivity values measured at a depth of 5 mm can be up to five times lower than those measured at 50 mm, this effect being due to drying action rather than hydration.

It can also be informative to present conductivity measurements in a dimensionless format by *normalising* all conductivity values by the value obtained at a depth of 50 mm, i.e., $N = \sigma_t/\sigma_{t,50}$ where N is the normalised conductivity; σ_t is the conductivity across a particular electrode pair at time, t, after the start of the initial absorption test, and $\sigma_{t,50}$ is the value of conductivity across the electrode pair positioned at 50 mm, also at time, t. The N curve at 50 mm will thus be a horizontal line with a value of 1.0. The 50-mm depth was chosen to benchmark all conductivity values since, as noted above, it primarily reflects hydration effects, and is not influenced to any great extent by surface wetting and drying or NaCl ingress (at this early stage).

Figs. 10 and 11 present N over the test period for, respectively, water- and NaCl-exposed samples. Wetting and drying cycles are still clearly evident; however, the most striking effect is the influence of NaCl on N in comparison to the respective water-exposed specimens, particularly over the surface 0–10 mm. This feature is not so pronounced on the respective conductivity versus time response presented in Figs. 8 and 9.

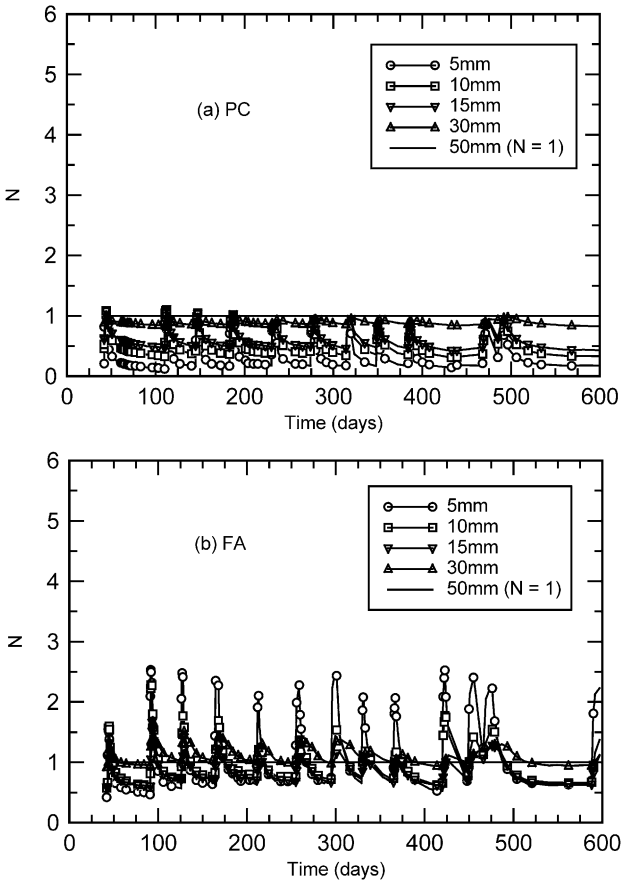

Fig. 10. Change in N during cyclic wetting and drying with water applied at the exposed surface for (a) PC mix and (b) FA mix.

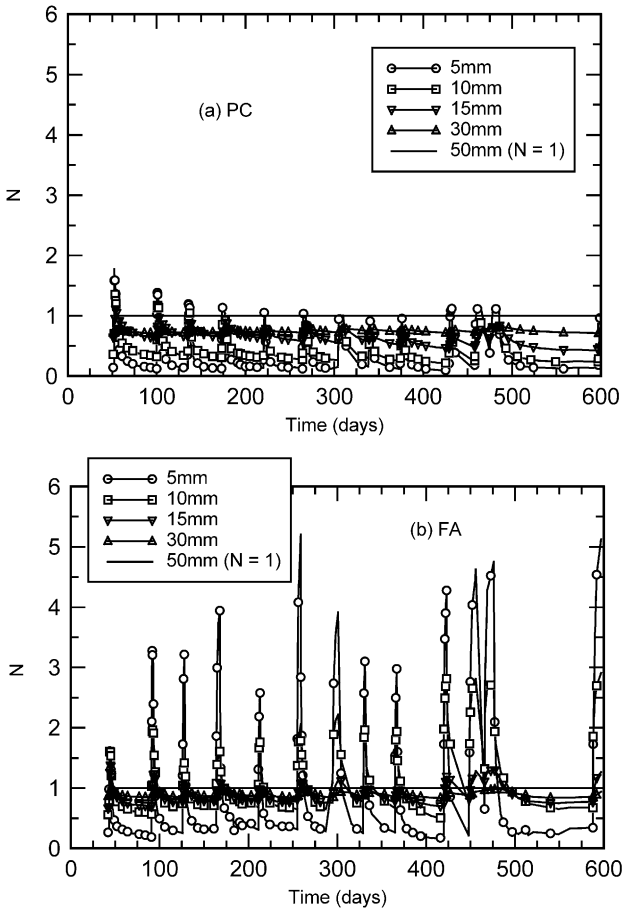

Fig. 11. Change in N during cyclic wetting and drying with 1.0 M NaCl solution applied at the exposed surface for (a) PC mix and (b) FA mix.

Two processes will, in the main, influence conductivity:

1. hydration, pozzolanic reaction, chloride binding (formation of Friedel's salt) and drying effects all serving to decrease conductivity; and,
2. water ingress increasing conductivity, enhanced by the presence of NaCl within the invading solution.

Once hydration and pozzolanic activity have ceased, conductivity will be a function of both level of pore saturation and pore-fluid conductivity. If the level of saturation fluctuates due to cycles of wetting (with water) and drying, the conductivity will change in sympathy; if monitored over time, the conductivity will tend to fluctuate about a zone defined by the maximum/minimum values after wetting/drying respectively, this zone remaining relatively constant. This is evident in Fig. 10 for both sets of water-exposed samples. The water-exposed FA (Fig. 10(b)) dis-

Fig. 12. Marine exposure site: concrete specimens at low-water-mark position.

plays N values at 5 mm, which consistently peak above the benchmark value of 1.0 (at 50 mm). This feature is associated with a more porous surface zone due to the susceptibility of this replacement material to curing conditions.

When the invading water contains dissolved salt, then cycles of wetting and drying will cause the conductivity to fluctuate between a zone which gradually increases with time as each electrode pair responds to the increasing NaCl concentration in the pore water. This is evident in Fig. 11 towards the end of the period presented. N values indicate ionic ingress into the surface 0–5 mm for the PC mix (Fig. 11(a)); the FA mix (Fig. 11(b)) on the other hand, shows enrichment of the surface 0–10 mm. As the NaCl advances into the covercrete the conductivity, hence N, at each pair of electrodes will increase in response to the increasing ionic concentration within the pore fluid. This allows tracking of the chloride front.

2.3.2.2. Marine exposure site. Concrete blocks were secured in galvanised steel frames and positioned at three locations (a) just above the low water mark; (b) just below the high water mark and (c) well above the high water mark. The low-water mark position, for which data are presented, is shown Fig. 12. At this position, the blocks were submerged during most of the tidal cycle and subjected to a maximum hydrostatic head of approximately 2.5 m at full tide. Fig. 13 displays the change in conductivity within the covercrete at the depths indicated for Mix 1 (Fig. 13(a)) and Mix 3 (Fig. 13(b)) at depths indicated. Apart from the initial 2–3 weeks exposure, conductivity values for the FA mix are noticeably lower than the PC mix; further, the FA mix displays a more discernible decrease and attributed to the pozzolanic reaction. Regarding the latter, at the end of 2 years exposure, the conduc-

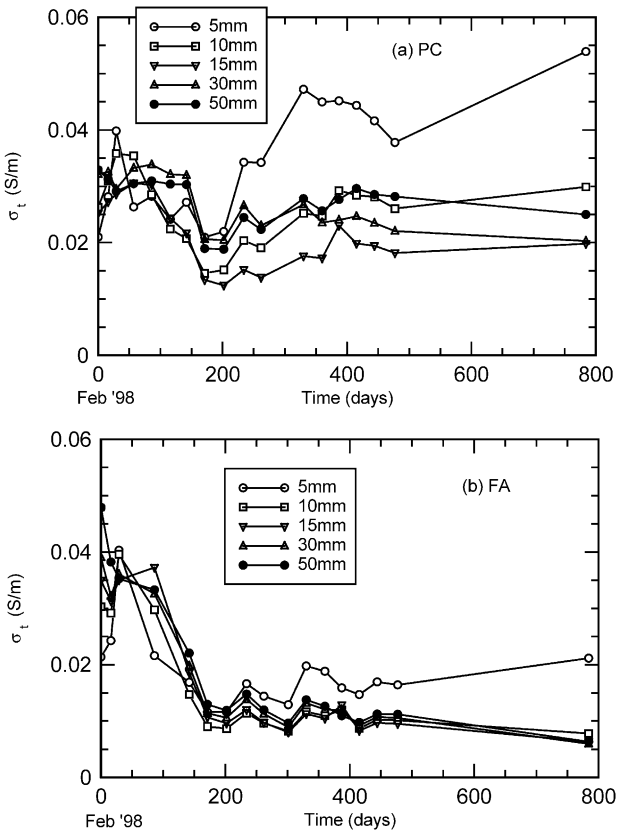

Fig. 13. Change in conductivity for (a) PC mix and (b) FA mix at low-water-mark position.

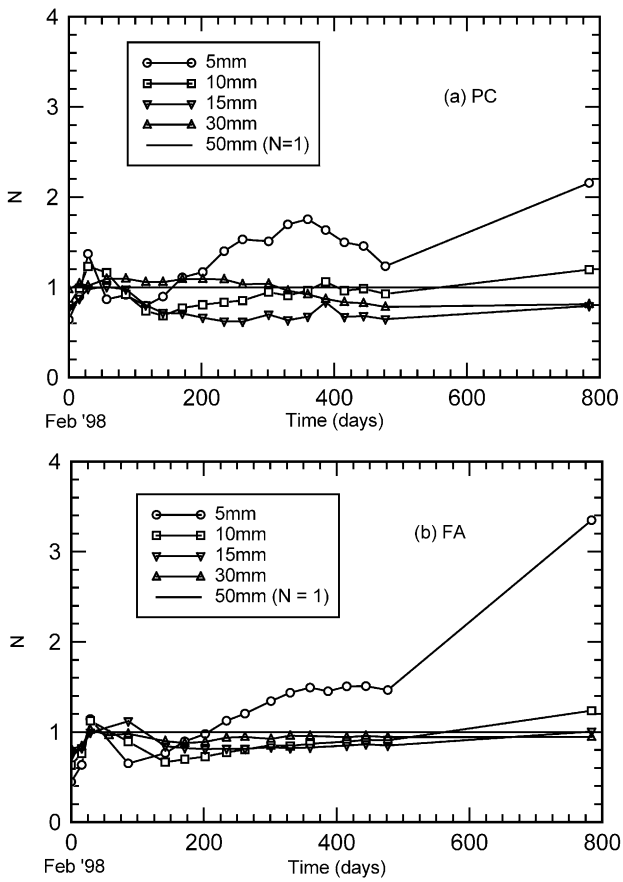

Fig. 14. Change in N for (a) PC mix and (b) FA mix.

tivity of the concrete at a depth of 50 mm is approximately 2.5×10^{-2} S/m (40 Ω m) for the PC specimens and 7×10^{-3} S/m (143 Ω m) for the FA blocks.

Fig. 14 presents the normalized conductivity values, *N*. In this format, *N* values at 5 mm for both mixes show a continual increase after approximately 100 days exposure, although this is more significant in the case of the FA mix. This would signify that sufficient quantities of ions have now reached the 5-mm electrode level to alter the pore-water conductivity. Changes in pore-fluid conductivity are thus exerting a greater influence on concrete conductivity than microstructural changes due to hydration/pozzolanic reaction. At 600 days exposure, *N* values at 10 mm also begin to increase above the benchmark value of 1.0, although, at this stage, it is not as significant. This trend, namely, that the FA mix displays *N* values greater than the PC mix in the surface 5 mm, is similar to that obtained from laboratory specimens.

It would be anticipated that, with time, as ions from the seawater penetrate the covercrete, each electrode pair will, in sequence, display an *N* value which increases with time.

3. Concluding comment

Through a series of research programs, it has been shown that EP measurements can be used as an investigative technique in the study of cementitious systems at both the micro- and macroscale. Both fixed-frequency and spectral measurements were exploited in this respect and data can be presented in a number of formalisms: complex impedance; capacitance/dielectric constant and conductance/conductivity. A number of other features are also of importance: the method is nondestructive; samples need not be restricted to cement pastes as mortars and concretes can also be studied, in addition, measurement can be taken while the material is in the liquid or hardened state. The testing methodology also lends itself to continuous real-time monitoring of concrete.

Acknowledgements

The authors wish to thank the Engineering and Physical Sciences Research Council (EPSRC), United Kingdom, for financial support (research grants GR/L55810, GR/N16365, GR/R42993).

The work relating to the outdoor exposure sites forms part of the Transport Research Laboratory (UK) programme into monitoring and improving the performance of structural concrete in bridges undertaken for the Scottish Executive Development Department (SEDD) (Bridges Section). Funding from the SEDD is gratefully acknowledged. The views expressed in this paper are those of the authors and not necessarily those of the National Roads Directorate, in this respect.

Thanks are also expressed to Dr. J. Beaudoin at the Canadian National Research Centre and Dr. L. Sear at the United Kingdom Quality Ash Association for the supply of fly ash samples.

References

[1] W.J. McCarter, S. Garvin, N. Bouzid, Impedance measurements on cement paste, J. Mater. Sci. Lett. 7 (1988) 1056–1057.
[2] W.J. McCarter, R. Brousseau, The A.C. response of hardened cement paste, Cem. Concr. Res. 20 (6) (1990) 891–900.
[3] K. Brantervik, G.A. Niklasson, Circuit models for cement based materials obtained from impedance spectroscopy, Cem. Concr. Res. 21 (4) (1991) 496–508.
[4] P. Gu, P. Xie, J.J. Beaudoin, R. Brousseau, AC impedance spectroscopy: I. A new equivalent circuit model for hydrated Portland cement paste, Cem. Concr. Res. 22 (5) (1992) 833–840.
[5] P. Gu, P. Xie, Z. Xu, J.J. Beaudoin, A rationalized AC impedance model for microstructural characterisation of hydrating cement systems, Cem. Concr. Res. 23 (2) (1993) 359–367.
[6] R.T. Coverdale, E.J. Garboczi, H.M. Jennings, B.J. Christensen, T.O. Mason, Computer simulation of impedance spectroscopy in two dimensions: application to cement paste, J. Am. Ceram. Soc. 76 (6) (1993) 1153–1160.
[7] R.T. Coverdale, B.J. Christensen, T.O. Mason, H.M. Jennings, E.J. Garboczi, Interpretation of the impedance spectroscopy of cement paste via computer modelling: dielectric response, J. Mater. Sci. 9 (1994) 4984–4992.
[8] B.J. Christensen, R.T. Coverdale, R.A. Olsen, S.J. Ford, E.J. Garboczi, H.M. Jennings, T.O. Mason, Impedance spectroscopy of hydrating cement-based materials: measurement, interpretation, and applications, J. Am. Ceram. Soc. 11 (77) (1994) 2789–2804.
[9] E.J. Garboczi, L.M. Schwartz, D.P. Bentz, Modelling the D.C. electrical conductivity of mortar, Mater. Res. Soc. Symp. Proc. 370 (1995) 429–436.
[10] X. Lu, Application of the Nernst–Einstein equation to concrete, Cem. Concr. Res. 2 (27) (1997) 293–302.
[11] J.B. Hasted, Aqueous Dielectrics, Chapman & Hall, London, 1973 (302 pp.).
[12] Z. Huanhai, W. Xuequan, X. Zhongzi, T. Mingshu, Kinetic study on hydration of alkali-activated slag, Cem. Concr. Res. 6 (23) (1993) 1253–1258.
[13] C. Shi, R.L. Day, A calorimetric study of early hydration of alkali-slag cements, Cem. Concr. Res. 6 (25) (1995) 1333–1346.
[14] X. Zhang, Microwave study of hydration of slag cement blends in early period, Cem. Concr. Res. 5 (25) (1995) 1086–1094.
[15] British Standards Institution, London, BS 3892-1, Pulverised-fuel ash. Specification for pulverised-fuel ash for use with Portland cement, 1997.
[16] W.J. McCarter, G. Starrs, T.M. Chrisp, Immittance spectra for Portland cement/fly-ash based binders during early hydration, Cem. Concr. Res. 29 (1999) 377–387.
[17] E. Nagale, U. Schneider, Fly-ash determination in fresh concrete using flotation, in: H.W. Reinhardt (Ed.), Proceedings International RILEM Workshop, Mainz, Germany, March (1990) 40–48.
[18] W.J. McCarter, M. Emerson, H. Ezirim, Properties of concrete in the cover zone: developments in monitoring techniques, Mag. Concr. Res. 47 (172) (Sept. 1995) 243–251.
[19] W.J. McCarter, M. Emerson, H. Ezirim, Properties of concrete in the cover zone: water penetration, sorptivity and ionic ingress, Mag. Concr. Res. 48 (176) (Sept. 1996) 149–156.
[20] T.M. Chrisp, G. Starrs, W.J. McCarter, L. Rouchatas, J. Blewett, Temperature–conductivity relationships for concrete: An activation energy approach, J. Mater. Sci. Lett. 2001 (20) 1085–1087.